Synergy effect of *Urtica dioica* and ZnO NPs on microstructure, antibacterial activity and cytotoxicity of electrospun PCL scaffold for wound dressing application

Yasaman Ghiyasi [a], Esmaeil Salahi [a],*, Hamid Esfahani [b],*

[a] *Ceramic Department, Materials and Energy Research Center (MERC), Karaj, Iran*
[b] *Department of Materials Engineering, Bu-Ali Sina University, Hamedan, Iran*

ABSTRACT

This study focuses on the synergy effect of *Urtica dioica* as a natural medicinal plant and ZnO nanoparticles (NPs) as a common and active antibacterial metal oxide on the microstructure, composition, mechanical properties, hydrophobicity, antibacterial activity, and fibroblast cell cytotoxicity of biocompatible polycaprolactone (PCL) scaffolds. The nanostructured fibrous pristine and hybrid scaffolds were provided using the electrospinning method. The microstructure of scaffolds was characterized using FESEM, EDS, FTIR. The results indicated that the incorporation of *Urtica dioica* and ZnO NPs have a significant impact on the morphology and molecular bond groups of the PCL scaffold. The evaluation of the strain-stress curve of scaffolds depicted that the incorporation of *Urtica dioica* enhances the tensile strength from 1.52 MPa to 2.54 MPa. The incorporation of *Urtica dioica* and ZnO NPs improves the water uptake ability, regulates the water affinity between hydrophobicity-hydrophilicity and controls the release of *Urtica dioica*. The hybrid composition made the highest antibacterial hybrid scaffold against *E. coli* and *S. aureus*. Cell cytotoxicity studies using fibroblast L929 cells also showed that the highest cell viability (97.8 %) is for a hybrid *Urtica dioica* and ZnO scaffold where the proper cell adhesion to fibers of the scaffold with a polar shape morphology occurs. Our findings suggest that incorporation of 4 wt.% of *Urtica dioica* and 1 wt.% of ZnO NPs to PCL scaffold leads to the best properties for wound dressing application.

1. Introduction

Wound dressing is one of the most advanced techniques to treat skin injuries [1]. Among the various skin injuries, diabetic ulcers have long-lasting and painful side effects and must be seriously treated [2]. An advanced wound dressing biomaterial should be capable of overcoming chronic long-term inflammation, microbial and bacterial infection, impaired growth factor secretion and angiogenesis, impaired collagen anabolism, poor migration and translocation of fibroblasts and keratinocytes, excessive secretion of degradative enzymes, and non-information vessels and extracellular context defects [3,4]. To have an accelerated wound healing process, a system with parameters such as proper mechanical wound protection, high water uptake ability to provide the humidity for the wound, high porosity for gas exchange, non-toxicity, and antibacterial activity should be designed [5,6]. Also, it has been suggested that a wound dressing scaffold provides the free pathways for migration of various growth factors such as important fibroblasts. The fibroblasts supply the tensile strength within the wound via the formation of the cross-linked collagen fibers by deposition on the extracellular matrix (ECM) [7,8].

Among the various technologies in the development of wound dressing systems, nanofibrous scaffolds have drawn attention because of their high similarity to the natural ECM. Also, nanofibrous scaffolds have excellent mechanical properties and allow a proper gas exchange [9]. The electrospinning method is the most widely used method for producing a nanofibrous scaffold [10]. This method has the flexibility to produce fibers with diversity in synthetic and natural polymers. This method provides scaffolds with high porosity, high surface to volume ratio, and oxygen-permeable with excellent mechanical properties and a similar structure to the natural ECM easily and with a low cost [11–13]. The monolithic and composite nanofibrous scaffolds can be easily produced by the electrospinning method [14,15].

There are different biopolymers with essential factors for wound dressing applications. However, polycaprolactone (PCL) with a semi-

---

crystalline microstructure, high mechanical flexibility, inherent non-toxicity, low biodegradability, high biocompatibility, and high mimicking the ECM is widely used as the matrix in many biomedical applications [16,17]. Furthermore, the low hydrophilic nature of PCL which affects the adhesion and cell proliferation makes this biopolymer a unique choice [18,19].

Zinc oxide (ZnO) is one of the metal oxide groups that received attention for its antibacterial activity [20]. ZnO in a nano-scale presented higher antibacterial behavior because of the higher amount of zinc ions on the surface for improving re-epithelialization, reducing the inflammation and bacterial growth, as well as recovery of ECM [21,22]. It should be emphasized that the ZnO nanoparticles (NPs) are relatively inexpensive, biocompatible, and have low toxicity compared to other metal oxide NPs [23]. Hence, ZnO NPs are used to enhance the antibacterial activity in the electrospun scaffolds. Münchow et al. [24], used the ZnO NPs in electrospun scaffold and found that not only antibacterial properties enhanced, but also cell proliferation and wound healing improved. Ahmed et al. [4], found that by the incorporation of ZnO NPs, the antibacterial activity, antioxidant potential and wound healing rate of the polyvinyl alcohol (PVA)/chitosan nanofibers (NFs) improved. By the further inspection of the role of the ZnO NPs inside the PCL NFs by Augustine et al. [25], it was found that the angiogenesis increased and large numbers of blood vessels with many branches were observed.

Urtica dioica is a well-known medicinal plant that contains significant amounts of flavonoids, chlorophylls, carotenoids and their derivatives, minerals such as iron, proteins, oils, organic acids, and essential vitamins. *Urtica dioica* has various biological properties and is endemic to Europe, North Africa, North America, Asia, and north of Iran [26]. It is worth mentioning that *Urtica dioica* has antibacterial, antioxidant, anti-inflammatory, anti-viral, and anti-ulcer properties due to its phenolics and flavonoids structure [26,27]. Moreover, the histamine agent in the leaves of *Urtica dioica* may accelerate the wound healing process [28]. Up to now, the antibacterial activity of *Urtica dioica* against resistant to methicillin-resistant *Staphylococcus aureus* and methicillin-sensitive *Staphylococcus aureus* has been approved [29]. Babaei et al. [30] observed that *Urtica dioica* has strong wound healing properties and increases the number of fibroblast cells in the wound site.

The novelty of the present study is the synthesis of a hybrid nanostructured scaffold for wound dressing applications made by a natural compound (i.e. *Urtica dioica*) which has the advantages of the common PCL-based scaffolds and improves the wound dressing properties such as microstructure, mechanical properties, wettability, antibacterial and cytotoxicity behaviors. This study aims to investigate the effect of *Urtica dioica* and ZnO NPs as an individual additive and also as combined additives on the wound dressing application of PCL-based scaffold. Hence, the ZnO NPs were synthesized using the sol-gel method, and PCL pristine and hybrid scaffolds were produced using the electrospinning method. The synergy effect of *Urtica dioica* and ZnO NPs on the essential factors of a wound dressing scaffold including its morphology, chemical and antibacterial activity, hydrophobicity and fibroblast cell cytotoxicity was studied.

2. Materials and methods

2.1. Materials

To prepare the scaffolds, polycaprolactone (PCL) (Sigma–Aldrich, $M_w = 80000$, No. 440744), *Urtica dioica* (U, Barij essence company, herbarium number; 240-1), zinc acetate dehydrate (Merck, No. 5970-45-6), sodium hydroxide (Sigma–Aldrich, No. 1310-73-2), N, N-dimethylformamide (DMF, Sigma–Aldrich, No. 227056), and dichloromethane (DCM, Sigma–Aldrich, No. 75-09-2) were purchased.

2.2. Synthesis of ZnO NPs

To prepare the ZnO NPs, zinc acetate dihydrate (Zn $(CH_3COO)_2.2H_2O$) was dissolved in deionized water with a concentration of 0.02 M via stirring the solution at 35 °C. Then 80 mM of sodium hydroxide (NaOH) solution was added to the initial solution dropwise 2.5 mL.min^{-1} over 60 min. The temperature was set at 35 °C and the solutions were stirred for 2 h to obtain a milky solution. To obtain solid ZnO NPs, the solution was filtered using a centrifuge at 3000 rpm and sediments were washed several times with deionized water. Then the resulting powders were dried in the oven at 80 °C for 80 h. Finally, the powders were heat-treated at 400 °C for 2 h in air atmosphere. The heating rate was 10 °C.min^{-1} and cooling was performed slowly in the furnace.

2.3. Scaffold preparation

To prepare PCL/*Urtica dioica*/ZnO scaffolds, at first, 1% w/v of ZnO NPs was dissolved in DMF/DCM (1:4). The suspension was stirred for several hours and then PCL (14 % w/v) and U (4% w/v) were added to the solution. The mixture was again stirred for 24 h to obtain a homogeneous solution. Similar solutions were separately provided with 2% and 4% w/v of ZnO NPs. The obtained solutions were injected into a 3 ml plastic syringe attached to a 22 G stainless steel needle. The viscosity of electrospun solutions was measured by Ubbelohde viscometer. The electrospinning process was carried out at 10 kV (DC) high voltage, 0.6 mL.h^{-1} feeding rate, and a distance of 10 cm between needle tip to an aluminum collector. The collected mats were dried under the vacuum condition to completely remove the solvent. For further investigations, samples were cut to appropriate dimensions and they were coded as shown in Table 1.

2.4. Characterization of scaffolds

The morphology of the ZnO powders and electrospun scaffolds was studied using a field emission scanning electron microscope (FESEM, MIRA3-TESCAN) equipped with an energy dispersive spectroscope (EDS) analyzer. The EDS spectra were provided for all samples to investigate the elemental composition. ImageJ software (1.38x NIH USA) was employed to measure the size and size distribution of particles and fibers. To ensure the accuracy of the result, the diameters of 70–100 fibers of each scaffold were measured and their mean size and size distribution were reported. The dynamic light scattering (DLS) technique was applied by a device (HORIBA SZ-100 model) to measure the size distribution and polydispersity index (PDI) of ZnO NPs. The surface porosity of electrospun scaffolds was calculated from the FESEM images using ANIX software (Iran, version 1.5). The functional molecule groups of pristine and hybrid scaffolds were analyzed by a Fourier transform infrared (FTIR) spectrometer (Perkin-Elmer) in the range of 400–4000 cm^{-1}.

2.5. Mechanical properties of scaffolds

The tensile strength of scaffolds was measured using a uniaxial tensile testing machine (SANTAM, STM-1). Scaffolds with dimensions of 15 × 30 mm^2 were subjected to a 10 N tensile force with a 1 mm.min^{-1}

Table 1
Sample code, composition, and viscosity of solutions for electrospinning procedure.

Sample Code	Polycaprolactone (P) Wt. %	Urtica dioica (U) Wt. %	ZnO NPs (Z) Wt. %	Viscosity cP
P	14	–	–	450
PU	14	4	–	480
PZ1	14	–	1	439
PUZ1	14	4	1	376
PUZ2	14	4	2	350
PUZ4	14	4	4	328

tensile rate until the failure of samples. Also, Young's modulus, yield strength, and elongation of the scaffolds were calculated.

2.6. Wettability of scaffolds

To determine the water uptake ability of all scaffolds, the weight of the dried sample (W_d) was measured. Over 1, 3, and 7 days of immersion in 5 ml of phosphate-buffered saline (PBS) at 37 °C, the weight of the soaked sample (W_s) was measured. The water uptake percentage was calculated using the following equation [31]:

$$Water uptake = \frac{(W_s - W_d)}{W_d}.100 \tag{1}$$

Also, the surface wettability of the electrospun pristine and hybrid scaffolds was studied by measuring the water contact angle (WCA) of 4 μL distilled water droplets on the surface at 18 °C. The dynamic WCA was recorded for 1 min by a camera with the aid of a 2X lens and Protractor (AMCAP, VERSION 9.016) software-connected. To ensure the accuracy of the results, the experiment was repeated at 3 points of each sample and the mean value was reported.

2.7. In-vitro release of Urtica dioica and ZnO NPs from scaffolds

To investigate the release kinetic of *Urtica dioica* and ZnO NPs from the hybrid scaffolds, samples with an area of 1×1 cm^2 were immersed in 3 mL of PBS solution while stirring with 80 rpm at 37 °C in an incubator. The weight of samples was recorded before the immersion. 1 mL of solution was extracted at specified times (1, 3, and 7 days) to calculate the concentration of released *Urtica dioica* and ZnO NPs. The concentration of *Urtica dioica* and ZnO NPs was calculated based on Beer's law [32]. The UV–vis instrument (model; Photonix-Ar) was used to measure the absorbed intensity at $\lambda = 205$ nm for *Urtica dioica* and $\lambda = 355$ nm for ZnO NPs. The release amount (Q_R) (mg. g^{-1}) at particular times was calculated by substituting the values of released concentration (C_R) (mg.l^{-1}), specific volume of solvent (V), and initial weight (W_i) (g) of the scaffold in the Eq. 2.

$$Q_R = \frac{C_R.V}{W_i} \tag{2}$$

The release parentages of the maximum amount of encapsulated *Urtica dioica* and ZnO NPs were also calculated assuming a 4 Wt.% of *Urtica dioica* and 1, 2, and 4 Wt.% of ZnO NPs.

2.8. The antibacterial property of scaffolds

The antibacterial behavior of the pristine and hybrid scaffolds was evaluated by the plate count method using *Escherichia coli* gram-negative bacteria (*E. coli*) and *Staphylococcus aureus* gram-positive bacteria (*S. aureus*). From the fresh bacteria, culture provides suspension containing a half MacFarland concentration (1.5×10^8 CFU. ml^{-1}) and the re-concentration (1.5×10^6 CFU. ml^{-1}) was prepared. The scaffolds were cut into 1×1 cm^2 and both sides were sterilized for 1 h by UV irradiation before contact with bacterial suspension. After 5 days of culture, scaffolds were incubated for 48 h at 37 °C. Finally, the antibacterial activity of the scaffold was evaluated by photos taken from sample containers and the following equation [17].

$$Antibacterial activity = (1 - \frac{OD_2}{OD_1}).100 \tag{3}$$

Where OD_1 is the apparent density of the control solution and OD_2 is the apparent density of the scaffold solution.

2.9. Cytotoxicity of scaffolds

To evaluate the biocompatibility of pristine and hybrid scaffolds,

MTT cytotoxicity assay was performed using animal L929 fibroblast cells. Before the test, scaffolds were cut to 1×1 cm^2 and sterilized by UV irradiation for 20 min. After that, L929 cells were incubated in the scaffold at 5×10^5 cell. ml^{-1} for 3 h to completely adhere to the scaffold surface, then 1 mL of culture solution was added and incubated for 24 h at 37 °C with a humidity of 90 %. After 24 h, the culture media was removed and 1 mL of each media containing 10 % MTT solution was added to each well and then incubated for 4 h in darkness at 37 °C to form the formazan crystals. The whole MTT medium was then removed and 1 mL of dimethyl sulfoxide (DMSO) solvent was added to dissolve the produced blue crystals. After complete dissolution, the optical density (OD) value of the solution was recorded by UV–vis spectrophotometer at $\lambda = 560$ nm. The viability percentage of the scaffold was calculated using the following equation [33];

$$Validity(\%) = (\frac{OD_C}{OD_R}).100 \tag{4}$$

Where OD_c is the optical absorption of the synthesized scaffold and OD_R is the optical absorption of the control sample.

Before the cell attachment assay, samples with an area of 1×1 cm^2 were exposed to UV for 20 min and then transferred to 6-well plates. The 10^5 numbers of L929 cell were incubated with 1 mL of culture medium and left to adhere for 2 h. When the cells adhered, the fresh culture medium was added and allowed to stand 24 h. The cells were then fixed with 2.5 % glutaraldehyde solution. Finally, the samples were dehydrated by incremental concentrations of acetone (50, 60, 70, 80, 90, and 100 %) and were incubated in each acetone for 20 min. To study the cell morphology and its fixing to the scaffold, dried cellular constructs were observed by FESEM.

3. Results and discussion

3.1. The microstructure of ZnO NPs

The antibacterial activity of any ceramic crystalline NP depends on the particle and crystallite size and they affect the production of reactive oxygen species [34]. The morphology of ZnO NPs synthesized using the sol-gel method is shown in Fig.1 (a). As can be seen, homogenous spherical particles with a size smaller than 100 nm were obtained. The average size of ZnO NPs was 45.3 ± 9 nm. To ensure the purity of the synthesized ZnO NPs, XRD analysis was performed as presented in Fig.1 (b). According to the standard JCPDS card No. 01-079-0208 the hexagonal wurtzite ZnO structure was identified which belongs to the P63mc space group. Also, no other peaks were identified as the second phase which means that the obtained ZnO had a high purity. Moreover, the sharp peaks indicate the high crystalline nature of ZnO NPs. The crystallite size of (002) planes which have a significant role in antibacterial activity was calculated based on the Scherrer equation given in the following equation [35]:

$$d = \frac{0.9\lambda}{\beta.\cos\theta} \tag{5}$$

Where d is the crystallite size, λ is X-ray wavelength (1.54° A), β is the peak width at half height (FWHM), and θ is Bragg diffraction angle. According to the Scherrer equation, the average crystallite size of (002) planes was 60.5 nm confirming the nanostructure of ZnO NPs. Further investigation by the EDS technique was performed to evaluate the purity of ZnO NPs. Fig. 1 (c) confirms that Zn and O elements are the main components of ZnO NPs. Since the size and size distribution of ZnO NPs have a significant role in the electrospinning procedure, the DLS spectrum was provided for synthesized ZnO NPs. As shown in Fig. 1 (d), the spectrum presents that a narrow range of particles with an average size of 89.3 ± 5 nm forms the products. According to the results, PDI was obtained to be 0.5 indicating the homogeneous distribution of ZnO NPs. The nanostructure and homogeneous ZnO NPs can incorporate within
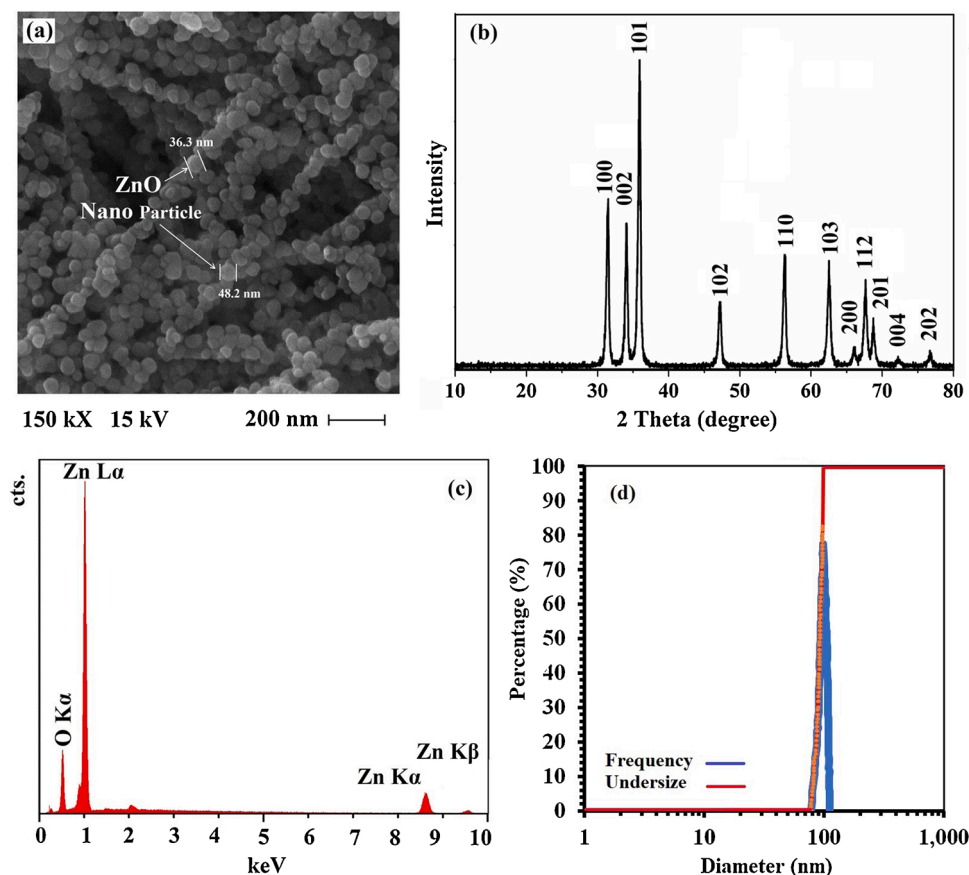
Fig. 1. (a) FESEM micrograph, (b) XRD pattern, (c) EDS spectrum, and (d) DLS spectrum of synthesized ZnO NPs.

the PCL fibers acting as the high potential sits for antibacterial behavior. Because the higher number of Zn atoms can be exposed to the surrounding texture for better antibacterial activity. Also, the high surface area per volume of synthesized ZnO NPs creates the high potential sites for the H_2O_2 production in the antibacterial process [34]. Therefore, it can be predicted that nanostructured ZnO NPs along with *Urtica dioica* inside the electrospun scaffolds have a synergetic effect on the antibacterial activity.

3.2. Microstructure and mechanical characterization of pristine and hybrid scaffolds

The arrangement, morphology, and size distribution of fibers throughout the scaffold, particularly in hybrid P-U-Z scaffolds, have significant effects on the physical and mechanical properties of a biocompatible scaffold. In spite of the composition, the rheology of the solution has a severe impact on the electrospinning process [10]. Hence, the viscosity of all solutions was calculated prior to the electrospinning procedure. As shown in Table 1, the results indicate that the addition of *Urtica dioica* and ZnO NPs causes the viscosity to increase and decrease, respectively. Fig. 2 presents the microstructure and chemical composition of pristine and hybrid scaffolds. As illustrated by microstructure graphs, the addition of *Urtica dioica* into PCL solution causes the fiber diameter size to decrease because of the plasticizer role of *Urtica dioica* with reconnection of polymer chains. The regulation of viscosity by incorporation of *Urtica dioica* resulted in a driving force for drawing more smooth fibers [36]. In contrast, the smooth fibers in P and PU scaffolds were replaced with larger and un-smooth fibers after the incorporation of ZnO NPs. The average size of fibers in pristine and hybrid scaffolds are compared in Table 2. Incorporation of higher amounts of ZnO reduced the uniformity and homogeneity of

microstructure and affected the open surface porosity of scaffold which has a significant impact on cell attachment and cell proliferation [37]. It should be noted that a porosity between 60–90 % is sufficient for tissue engineering performances in which the attached alive cells can breathe and also permeate the gases and wound dehydration can be prevented [38,39]. Generally, the electrospun scaffolds, known as the high porous materials with a porosity of more than 40 %, are highly suitable for tissue engineering [10]. Our findings revealed that the pristine and hybrid scaffolds have the required porosity for adhesion and cell proliferation during the tissue engineering applications. To explore the effect of *Urtica dioica* and ZnO NPs on the surface porosity, the open surface porosity of all scaffolds was measured. According to the surface porosity percentage given in Table 2, the PUZ1 scaffold had the highest surface porosity. EDS spectra provided from the surface of scaffolds confirm the polymeric nature of all scaffold matrices due to the sharp peaks of C and O. Moreover, identification of Zn peak in hybrid P-U-Z scaffolds confirms the incorporation of ZnO NPs.

To understand the effects of incorporation of *Urtica dioica* and ZnO NPs on the molecular groups of PCL scaffold, FTIR spectra were provided from P, PU, and PUZ scaffolds. According to the IR spectra shown in Fig.3, the main bands attributed to vibration bonds in PCL composition were identified at 2922 and 2859 cm^{-1} (CH_2 stretching), 1721 cm^{-1} (C═O stretching), 1238 and 1172 cm^{-1} (C—O—C stretching), and 1292 cm^{-1} (C—O and C—C stretching). Also, peaks at 1363, 1417, and 1462 cm^{-1} represent CH_2 band vibration, and a peak at 730 cm^{-1} is attributed to CH_2 rocking vibration [37,40]. The results confirmed the incorporation of *Urtica dioica* and ZnO NPs into PCL with the bands at 1063 and 2346 cm^{-1}, respectively [4,24,41]. It should be mentioned that the C—O—C alcohols, carboxylic acids, and esters found in the structure of the PU scaffold were not shifted by the incorporation of ZnO NPs. However, the CH stretching band at 2930 cm^{-1} was shifted to the 2936
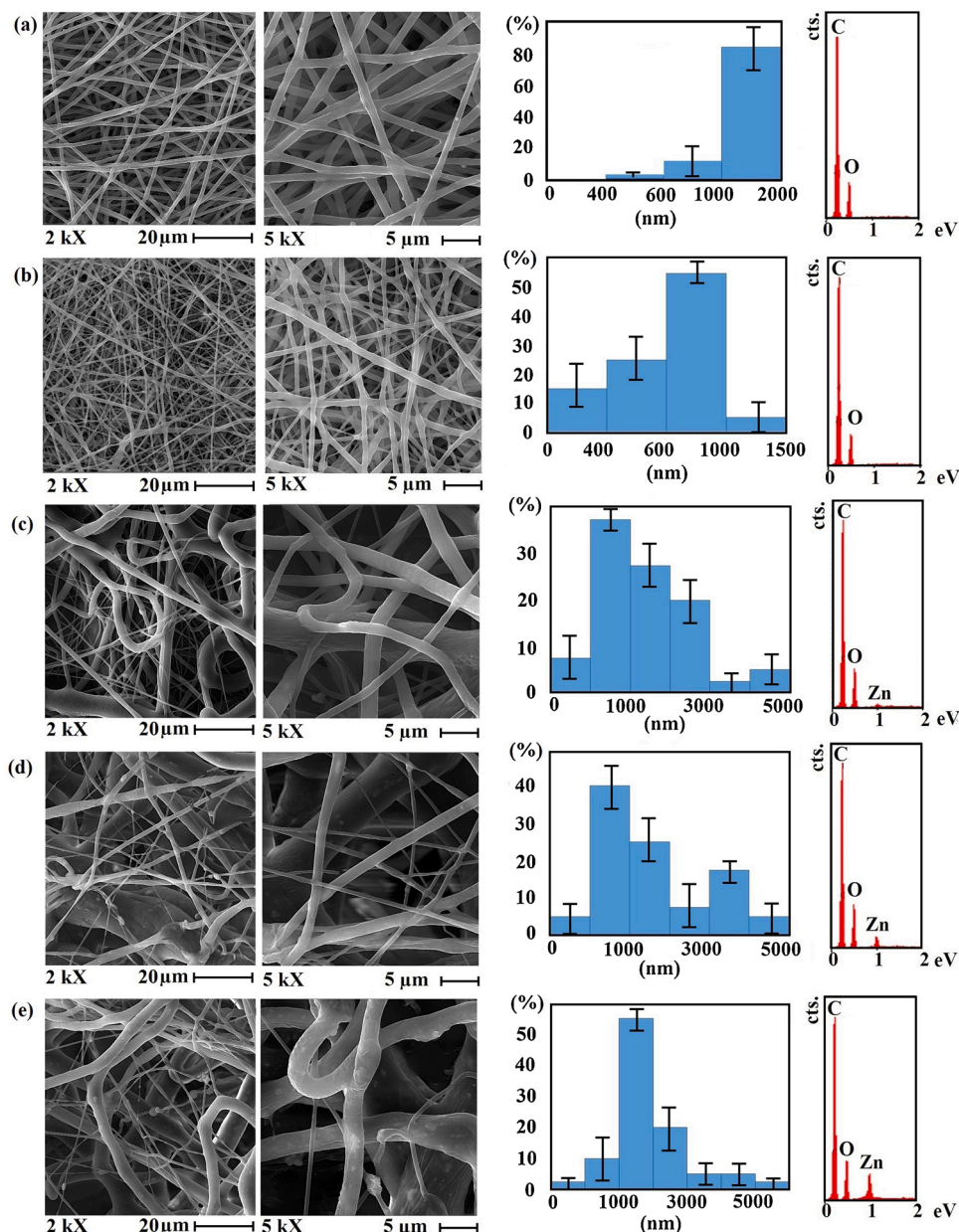
Fig. 2. FESEM micrograph in two magnifications of 2 kX and 5 kX, the size distribution of fibers and surface EDS of (a) P, (b) PU, (c) PUZ1, (d) PUZ2, and e) PUZ4 scaffolds.

Table 2
Physical and mechanical properties of scaffolds.

Sample Code	Physical properties		Mechanical Properties	
	Average size of fibers nm	Surface porosity %	Yield tensile strength MPa	Young's modulus MPa
P	1179 ± 25	45.6	1.52	10.24
PU	553 ± 49	56.6	2.54	15.34
PUZ1	1481 ± 180	66.3	0.85	3.37
PUZ2	1704 ± 300	47.3	1.54	12.10
PUZ4	1986 ± 250	33.9	0.72	4.26

cm^{-1}. Furthermore, ZnO incorporation tends to shift the stretching band of CH_2 in P and PU scaffolds to the higher frequencies representing the weaker bond in the PUZ1 scaffold.

A nanofibrous scaffold should exhibit appropriate mechanical

properties for wound dressing applications [42,43]. The stress-strain curve of pristine and hybrid electrospun scaffolds is presented in Fig.4 (a). The results indicated that the incorporation of *Urtica dioica* into the PCL matrix improved the tensile behavior. The Young's modulus and other mechanical properties of scaffolds are presented in Table 2. It should be mentioned that human skin has a complex and isotropic structure with nonlinear viscoelasticity. Therefore, different results have been reported for the mechanical properties of the skin. Generally, Young's modulus of the skin was reported to be between 0.42 and 0.85 MPa [44,45]. Our findings are in the range of 3.37–15.24 MPa which is much higher than the corresponding value for the skin. It was also found that the incorporation of *Urtica dioica* and ZnO NPs can improve the mechanical properties. There are two main reasons for the improvement of the mechanical properties of the PCL nanofibrous scaffold by the incorporation of *Urtica dioica*. The first one is the reduction of the fiber diameter in which leads to a better tensile strength because of the stronger adhesion between the fibers [18]. The second reason is the
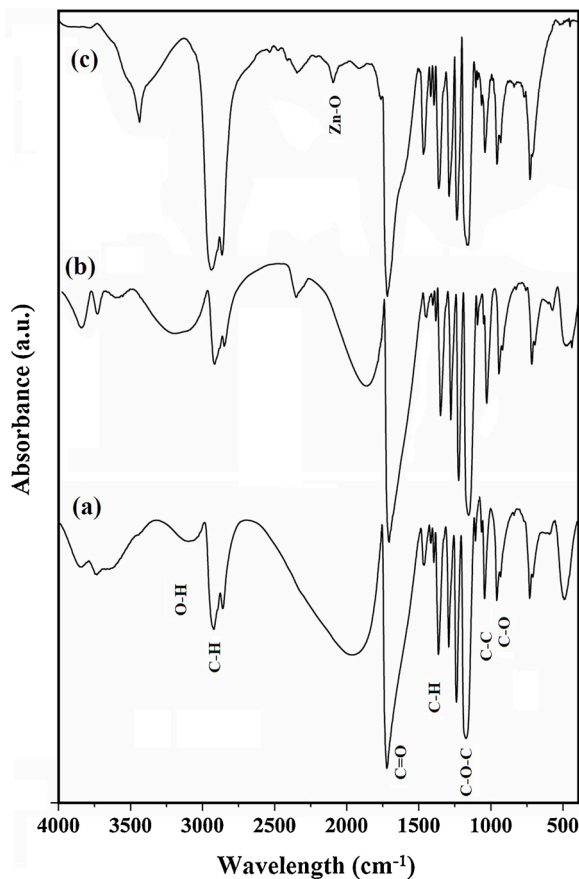
Fig. 3. FTIR spectra of P, PU, and PUZ2 scaffolds.

presence of hydroxyl groups in the chemical structure of *Urtica dioica* which enhances the hydrogen bonds between the hydroxyl groups and the functional groups of PCL standing out to the tensile forces [37]. In contrast to *Urtica dioica*, adding the ZnO NPs into the PU scaffold caused the mechanical properties to decline. The ZnO NPs act as a localized stress concentration within the fibers which is a common phenomenon for a rigid second phase [46]. Moreover, the ZnO NPs agglomerated during the synthesis process probably due to the high surface tension. Hence, the inappropriate distribution of ZnO NPs reduced the elasticity of PCL fibers. With higher amounts of ZnO NPs, stress concentrations increased. Therefore, the yield tensile strength and Young's modulus decreased in hybrid P-U-Z scaffolds. A typical agglomeration of ZnO NPs

is shown in Fig.4 (b). It is worth mentioning that the incorporation of ZnO NPs weakens the ester bonds in the PCL structure due to the weak Van Der Waals bonding between ZnO NPs and PCL. Our finding from FTIR analysis also confirmed that the incorporation of ZnO shifted the stretching band of CH_2 in PU scaffolds to higher frequencies representing the weaker bond in the PUZ1 scaffold.

3.3. Wettability of pristine and hybrid scaffolds

Since the hydrophobicity-hydrophilicity of a wound dressing scaffold should be known before application, the water uptake and wetting ability were measured for each scaffold. Fig. 5 (a) presents the water uptake percentage over 1, 3, and 7 days of immersion in PBS solution at the physiological conditions. The lowest value of water uptake was recorded for the pristine PCL scaffold even after 7 days of immersion in PBS solution. The hydrophobic nature of PCL polymer could prevent the penetration of water molecules to the scaffold. By incorporation of *Urtica dioica* in the PCL microstructure, the hydroxyl groups increased and also the crystalline regions decreased because of the softening of the PCL [36,41]. Hence, the water uptake percentage drastically increased up to 1660 % only after one day of immersion in the PBS solution. The results also showed that the incorporation of ZnO NPs enhances the water uptake ability of the hybrid P-U-Z scaffold such that approximately 3 times the ability of P scaffold was recorded for the PUZ1 scaffold. ZnO is hydrophilic in nature [42,43], so it could promote the penetration of water molecules to the scaffold. The weak Van Der Waals bonds between ZnO and PCL on one hand and the higher open surface porosity in P-U-Z scaffolds on the other hand resulted in higher percentages of water uptake.

Dynamic wetting ability was also performed using the contact angle of a droplet on the surface of scaffolds during 60 s (Fig.5 (b)) to identify the hydrophobicity-hydrophilicity of different scaffolds. The results confirmed the near-hydrophobic behavior for the pristine PCL scaffold due to the rather stable WCA values (78−65 °). The addition of hydroxyl groups to the P scaffold by incorporation of *Urtica dioica* modified the hydrophobic behavior. Although the initial WCA was 61°, the PU scaffold became super hydrophilic in less than 20 s. In contrast, the incorporation of 1 and 2 wt.% of ZnO NPs can regulate the water affinity between hydrophobicity-hydrophilicity which is favored for the adhesion of proteins and cells [47]. It seems to us that the Van Der Waals bonds between ZnO and PCL have complex effects on the OH^- groups made up by *Urtica dioica*, and therefore the hydrophobicity in P-U-Z increased in comparison to PU scaffold [48].

3.4. Urtica dioica and ZnO NPs release from hybrid scaffolds

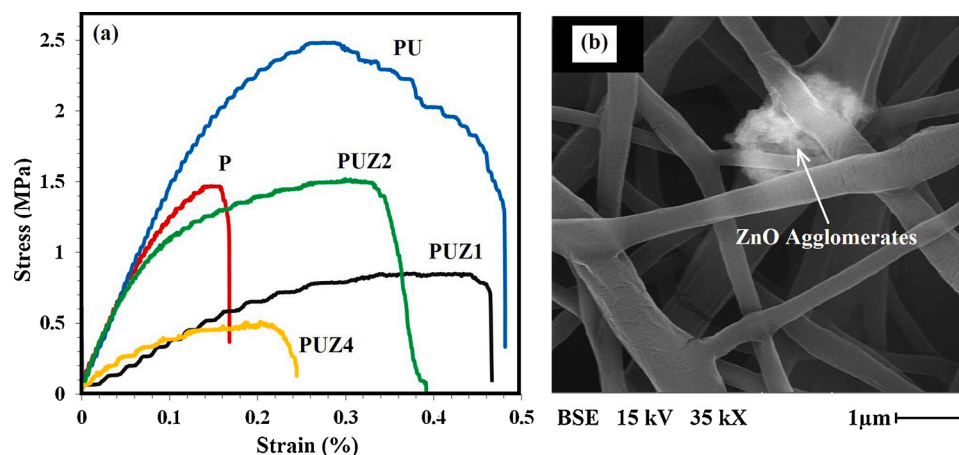The success of the antibacterial role of *Urtica dioica* agent depends on

Fig. 4. (a) The stress-strain curve of scaffolds, (b) a micrograph shows the ZnO agglomerates inside the fibers.
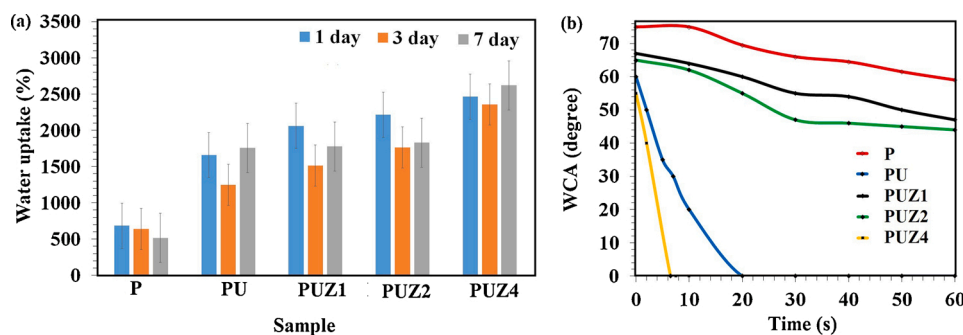
Fig. 5. (a) Water uptake percentage over 1, 3, and 7 days, (b) water contact angle of scaff ;olds during 60 s.

the kinetic release of *Urtica dioica* from hybrid scaffolds. Also, the stability of the ZnO NPs during the implantation has a critical role for a desirable scaffold because the excess release of the particles especially in the nano-scale may cause unknown reactions with the surrounding environment [49]. The release profiles of ZnO NPs and *Urtica dioica* from the hybrid scaffolds over 1, 3, and 7 days is presented in Fig. 6. The results showed that by the increase in the incorporation of ZnO NPs into the PCL scaffolds, the release amount of ZnO NPs increased. It was also found that the release profile of ZnO NPs was almost similar for each scaffold over different periods of soaking time indicating the stability of the hybrid scaffold. According to the release percentage of the maximum amount of encapsulated ZnO NPs, it can be assumed that the PUZ1 scaffold has the lowest release percentage (0.9 %) during the implantation which is appropriate for wound dressing applications [50]. In contrast, the release profile of *Urtica dioica* was completely different and showed a higher amount of release. Generally, the release of *Urtica dioica* enhanced at longer periods and the amount of incorporation of ZnO NPs had a complex effect on the release of *Urtica dioica*. The amount of released *Urtica dioica* over 1 day from PU scaffold was 14 mg.g^{-1} (36.3 %) which decreased to 13 mg.g^{-1} (33.0 %) and 6 mg.g^{-1} (17.1 %) for hybrid scaffold containing 1 and 2 wt.% of ZnO NPs, respectively. On the other hand, incorporation of more ZnO NPs (4 wt.%) increased the

release of *Urtica dioica* over one day, but also led to an uncontrollable increase in the release of *Urtica dioica* over 3 and 7 days. The release of *Urtica dioica* is controlled by the permeability of the PBS solution into the scaffold and leaking out of *Urtica dioica*. Our findings revealed that the highest percentage of water uptake was for the PUZ4 scaffold. Moreover, the mentioned scaffold became fully hydrophilic in less than 10 s. It seems that the solubility of *Urtica dioica* on the surface or inside the scaffold was regulated by incorporation of 1 and 2 wt.% of ZnO NPs because of the higher surface area to volume ratio. Therefore, it can be elucidated that incorporation of ZnO NPs up to 2 wt.% is adequate to control the release of *Urtica dioica* which has a significant role in medical treatments and especially the antibacterial activity for the wound dressing.

3.5. Antibacterial activity of pristine and hybrid scaffolds

The individual and synergy effects of *Urtica dioica* and ZnO NPs on the antibacterial activity of electrospun PCL scaffold were studied using the plate count method. Fig. 7 illustrates the activity percentage of pristine and hybrid scaffolds against *E. coli* and *S. aureus* over 5 days. The increase in antibacterial activity indicated that the incorporation of *Urtica dioica* into the PCL matrix can improve the antibacterial activity against *E. coli* and *S. aureus* by 47.3 % and 38.7 %, respectively. The presence of amino-base molecules (-NH$_2$) in *Urtica dioica* microstructure can react with the bacterial cell membranes and cause bacterial death [51]. This finding introduces the *Urtica dioica* as an effective natural antibacterial reagent for itself. The incorporation of ZnO NPs into the PCL matrix also demonstrated an improvement in the antibacterial activity against *E. coli* and *S. aureus* by 44 % and 76 %, respectively. The comparison of the individual role of *Urtica dioica* and ZnO NPs showed that the improvement of the antibacterial activity by *Urtica dioica* against *E. coli* is much higher than *S. aureus*. In contrast, ZnO NPs can kill *S. aureus* more than *E. coli*. It should be noted that the presence of lipopolysaccharide in the outer leaflet and phospholipids within the leaflet in the structure of cell walls of gram-negative bacteria results in
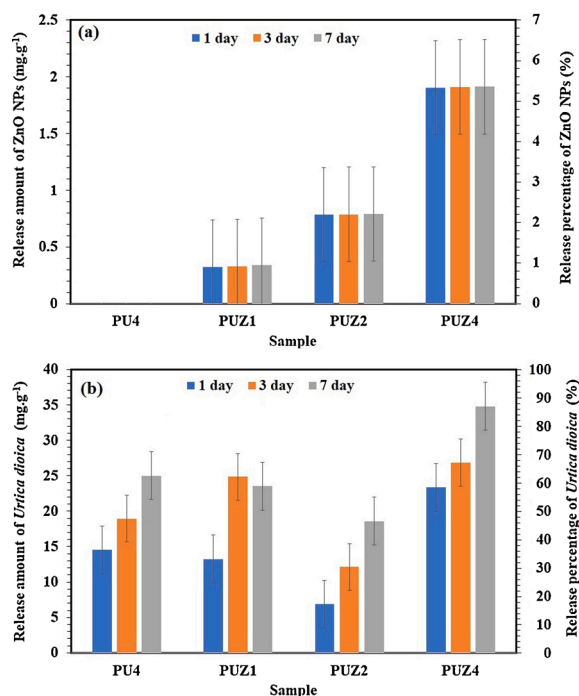

Fig. 6. Release amount (mg. g^{-1}) and release percentage (%) of (a) ZnO NPs and (b) *Urtica dioica* from scaffolds at different periods (1, 3, and 7 days).
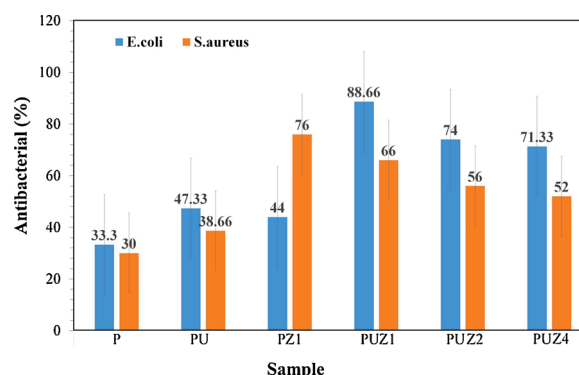

Fig. 7. The antibacterial activity of pristine and hybrid scaffolds over 5 days.

higher resistance against antibacterial reagents [46]. Therefore, *Urtica dioica* presents greater behavior than ZnO NPs.

The synergic effect of *Urtica dioica* and ZnO NPs on the antibacterial activity of electrospun PCL scaffold can be observed in P-U-Z scaffolds. With the incorporation of 4 wt.% of *Urtica dioica* and 1 wt.% ZnO NPs, the highest antibacterial activity against *E. coli* and *S. aureus* were obtained (88.7 % and 66 %, respectively). It seems that the corporation of *Urtica dioica* and ZnO NPs results in the formation of more reactive oxygen species which subsequently increases the antibacterial activity. Despite the presence of *Urtica dioica* in the scaffold, the antibacterial activity decreased with the incorporation of higher amounts of ZnO NPs because the reactive oxygen species can be harmful in the high amount of oxide NPs [11].

As shown in Fig.8, the optical photos of cell colonies incubated in agar plates demonstrate that the PUZ1 scaffold can further destroy *E. coli* and *S. aureus*. Further biocompatibility studies were performed on the PUZ1 scaffold to understand the effect of *Urtica dioica* and ZnO NPs on cell attachment and proliferation. It is worth mentioning that nanofibers containing herbal medicines with antibacterial potential can act as an effective drug delivery system especially for advanced wound dressing against common infections [52]. So far, various plant extracts are used on scaffolds. Also, the antibacterial properties of ZnO NPs have been proven in many studies [53,54].

3.6. Cytotoxicity assays of pristine and hybrid scaffolds

MTT assay was performed to evaluate the cytotoxicity of pristine and hybrid scaffolds using L929 cells over 1 day of cell culture using the indirect method. According to the OD values illustrated in Fig.9, no toxicity effect was observed for scaffolds. The results indicated that with the incorporation of *Urtica dioica* into the PCL matrix, viability increased from 91 % to 93 % which shows that *Urtica dioica* is a promising reagent for antibacterial activity and has an effective role in cytotoxicity behavior. Moreover, the incorporation of ZnO NPs could also improve the viability of L929 cells to 97.8 %. It seems that the synergy effect of *Urtica dioica* and ZnO NPs promoted the viability of L929 cells for proliferation and differentiation on the PUZ1 scaffold. Because the ZnO NPs have an effective role in the production stage of reactive oxygen species and *Urtica dioica* promotes cell adhesion by the hydrogen bonding groups [37]. Merrell et al. studied the wound dressing of PCL nanofibers with curcumin and found that with the addition of 3% curcumin, cell viability decreased from 90 % to 80 % [55], whereas in the present study the composition of *Urtica dioica* and ZnO NPs increased the cell viability from 91 % to 97.8 %.

The optical microscopic images of L929 cells on the pristine and hybrid scaffolds are presented in Fig. 10 (a–c). As can be seen, the proliferation of viable cells cultured on the PUZ1 scaffold is higher than
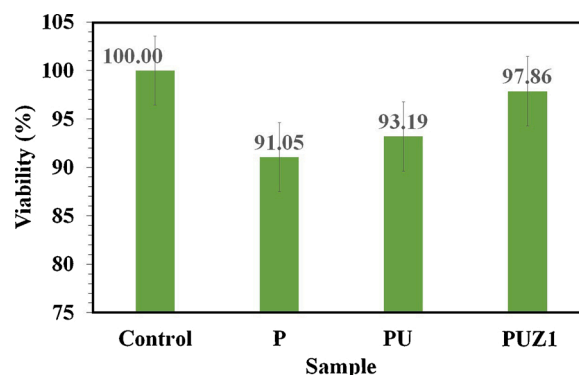
Fig. 9. L929 cell viability in control, P, PU, and PUZ1 scaffolds over one day of cell culture.

other scaffolds. Moreover, the morphology of cells changed from their spherical shape on the PCL scaffold by adding *Urtica dioica* within the fibers. The morphology of L929 cells also changed by the incorporation of ZnO NPs. The majority of alive cells on the PUZ1 scaffold had a spindle shape indicating its good biocompatibility. This finding confirms the fulfillment of the growth process of L929 cells on the PUZ1 scaffold [15].

The adhesion of fibroblast L929 on the pristine and hybrid scaffold was observed by FESEM micrographs. According to images shown in Fig. 10 (d–f), fibroblast L929 cells could properly attach to the surface of the pristine scaffold which indicates the good interaction between the PCL fibers and cells. With the incorporation of *Urtica dioica* and ZnO NPs, the morphology of cells and their adhesion model changed. The fibroblast L929 cells could properly anchor to the hybrid fibers, and they spread overlay on the top of the surface representing the higher viability which may be due to the improvement of the hydrophilic property and higher open surface porosity of the PUZ1 scaffold. The higher amount of hydroxyl groups generated by the incorporation of *Urtica dioica* could increase the adhesion strength of cells [56]. The presence of ZnO NPs on the surface of the hybrid scaffold had a significant role in the production of reactive oxygen species that accelerate the penetration of fibroblast L929 cells inside the scaffold [37]. Zadegan et al. studied the silk fibroin-*Urtica dioica* nanofibers and found that the cellular attachment improved with the addition of *Urtica dioica* [41].

Eventually, our findings suggest PUZ1 scaffold as the best candidate for wound dressing applications due to its optimum physical and mechanical properties, water affinity between hydrophilicity-hydrophobicity, high antibacterial activity, and appropriate cell proliferation and adhesion.
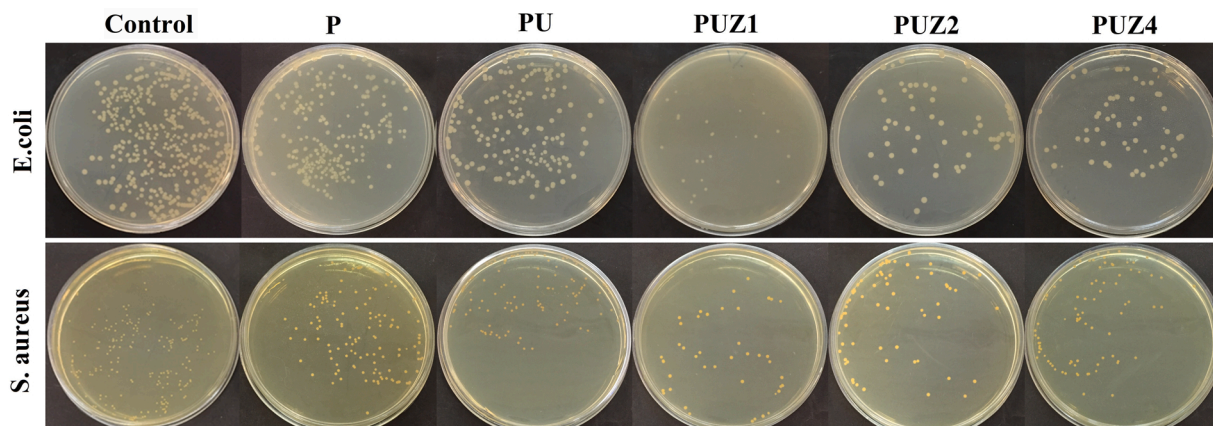
Fig. 8. The activity of control, pristine and hybrid scaffolds against *E. coli* (upper row) and *S. aureus* (bottom row) incubated in agar plates over 5 days.
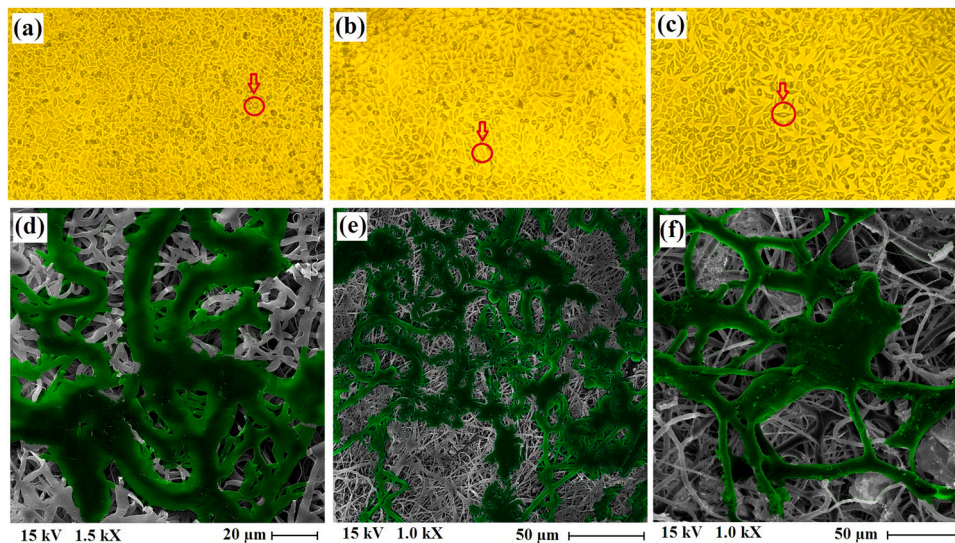
Fig. 10. Optical microscopic images (a, b, c), and FESEM micrographs (d, e, f) of L929 cells fixed on the P, PU, and PUZ1 scaffolds over 1 day. To present the adhesion of L929 cells to the scaffold, the cell body was marked by green color in the FESEM micrographs (For interpretation of the references to colour in this figure legend, the reader is referred to the web version of this article).

4. Conclusions

The hybrid scaffolds of PCL/*Urtica dioica*/ZnO NPs were synthesized using the electrospinning method. It was found that *Urtica dioica* and ZnO NPs were successfully incorporated into nanofibrous scaffolds. The incorporation of *Urtica dioica* and ZnO NPs had a countercurrent effect on the average size of fibers, *Urtica dioica* decreases, and ZnO NPs increase. FTIR spectra indicated that *Urtica dioica* did not significantly affect the molecular bond groups of PCL structure. However, ZnO NPs shifted CH and CH_2 bonds to higher frequencies representing the weaker bonds in P-U-Z scaffolds. The tensile strength and Young's modulus of PCL scaffolds decreased with higher incorporation of ZnO NPs, whereas *Urtica dioica* improved the mechanical properties. Both *Urtica dioica* and ZnO NPs increased the water uptake ability as individual and hybrid additives. Incorporation of 4 wt.% of *Urtica dioica* and 1 wt.% of ZnO NPs made a water affinity between hydrophobicity-hydrophilicity. The incorporation of the ZnO NPs up to 2 wt.% into the hybrid scaffold had a positive effect on regulating the release of *Urtica dioica*. The results confirmed that *Urtica dioica* has an antibacterial role. The hybrid composition of 4 wt.% of *Urtica dioica* and 1 wt.% of ZnO NPs presented the highest antibacterial activity against *E. coli* and *S. aureus*. Although the incorporation of *Urtica dioica* increased the cell viability approximately from 91 % to 93.2 %, the highest viability for fibroblast L929 (97.8 %). was observed for the hybrid scaffold with 4 wt.% of *Urtica dioica* and 1 wt.% of ZnO NPs. The incorporation of *Urtica dioica* changed the morphology of fibroblast L929 from spherical to square shapes, and by adding the ZnO NPs, it changed to two polar shapes. Cell cytotoxicity studies showed good cell adhesion to the fibers of the hybrid scaffold. Eventually, our findings suggest that *Urtica dioica* is a natural agent for improving the essential properties in wound dressing applications.

Data availability

The raw/processed data required to reproduce these findings cannot be shared at this time as the data also forms part of an ongoing study.

Declaration of Competing Interest

The authors declare that they have no known competing financial interests or personal relationships that could have appeared to influence the work reported in this paper.

References

[1] B. Joseph, R. Augustine, N. Kalarikkal, S. Thomas, B. Seantier, Y. Grohens, Recent advances in electrospun polycaprolactone based scaffolds for wound healing and skin bioengineering applications, Mater. Today Commun. 19 (2019) 319–335, https://doi.org/10.1016/j.mtcomm.2019.02.009.

[2] V. Vijayakumar, S.K. Samal, S. Mohanty, S.K. Nayak, Recent advancements in biopolymer and metal nanoparticle-based materials in diabetic wound healing management, Int. J. Biol. Macromol. 122 (2019) 137–148, https://doi.org/10.1016/j.ijbiomac.2018.10.120.

[3] F. Lv, J. Wang, P. Xu, Y. Han, H. Ma, H. Xu, Sh. Chen, J. Chang, Q. Ke, M. Liu, Zh. Yi, Ch. Wu, A conducive bioceramic/polymer composite biomaterial for diabetic wound healing, Acta Biomater. 60 (2017) 128–143, https://doi.org/10.1016/j.actbio.2017.07.020.

[4] R. Ahmed, M. Tariq, I. Ali, R. Asghar, P. Noorunnisa Khanam, R. Augustine, A. Hasan, International journal of biological macromolecules novel electrospun chitosan / polyvinyl alcohol / zinc oxide nano fi brous mats with antibacterial and antioxidant properties for diabetic wound healing, Int. J. Biol. Macromol. 120 (2018) 385–393, https://doi.org/10.1016/j.ijbiomac.2018.08.057.

[5] T. Thanh, N. Huynh, C. Khon, N. Thi, T. Hoai, B. Chi, Fabrication of electrospun polycaprolactone coated withchitosan-silver nanoparticles membranes for wound dressing applications, J. Mater. Sci. Mater. Med. 27 (2016) 156, https://doi.org/10.1007/s10856-016-5768-4.

[6] N.T. Thanh, M.H. Hieu, N.T. Minh Phuong, T.D.B. Thuan, H. Nguyen Thi Thu, et al., Optimization and characterization of electrospun polycaprolactone coated with gelatin-silver nanoparticles for wound healing application, Mater. Sci. Eng. C. 91 (2018) 318–329, https://doi.org/10.1016/j.msec.2018.05.039.

[7] N. Mohamed, N.G. Madian, Evaluation of the mechanical, physical and antimicrobial properties of chitosan thin films doped with greenly synthesized silver nanoparticles, Mater. Today Commun. 25 (2020) 101372, https://doi.org/10.1016/j.mtcomm.2020.101372.

[8] S.S. Behera, U. Das, A. Kumar, A. Bissoyi, A.K. Singh, Chitosan/TiO₂ composite membrane improves proliferation and survival of L929 fibroblast cells; Application in wound dressing and skin regeneration, Int. J. Biol. Macromol. 98 (2017) 329–340, https://doi.org/10.1016/j.ijbiomac.2017.02.017.

[9] J. Grip, R.E. Engstad, I. Skjæveland, J. Isaksson, P. Basnet, A. Mari, Beta-glucan-loaded nanofiber dressing improves wound healing in diabetic mice, Eur. J. Pharm. Sci. 121 (2018) 269–280, https://doi.org/10.1016/j.ejps.2018.05.031.

[10] H. Esfahani, R. Jose, S. Ramakrishna, Electrospun ceramic nanofiber mats today, materials. 10 (2017) 1238, https://doi.org/10.3390/ma10111238.

[11] M. Naseri-Nosar, S. Farzamfar, H. Sahrapeyma, S. Ghorbani, F. Bastami, A. Vaez, Majid salehi., Cerium oxide nanoparticle-containing poly (ε-caprolactone)/gelatin electrospun film as a potential wound dressing material: in vitro and in vivo evaluation, Materials Science and Engineering: C. 81 (2017) 366–372, https://doi.org/10.1016/j.msec.2017.08.013.

[12] M.R. Safaee-ardakani, A. Hatamian-zarmi, S. Mahdieh, Electrospun schizophyllan / polyvinyl alcohol blend nano fi brous scaffold as potential wound healing, Int. J. Biol. Macromol. 127 (2019) 27–38, https://doi.org/10.1016/j.ijbiomac.2018.12.256.

[13] R. Thomas, K.R. Soumya, J. Mathew, E.K. Radhakrishnan, Electrospun polycaprolactone membrane incorporated with biosynthesized silver nanoparticles as effective wound dressing material, Appl. Biochem. Biotechnol. 176 (2015) 2213–2224, https://doi.org/10.1007/s12010-015-1709-9.

[14] X. Liu, X. Wang, H. Ma, Sh. Venkateswaran, B.S. Hsiao, Colorful nanofibrous composite membranes by two-nozzle electrospinning, Mater. Today Commun. 21 (2019) 100643, https://doi.org/10.1016/j.mtcomm.2019.100643.

[15] R. Augustine, H.N. Malik, D.K. Singhal, A. Mukherjee, Electrospun polycaprolactone / ZnO nanocomposite membranes as biomaterials with antibacterial and cell adhesion properties, J Polym Res. 21 (2014) 347, https://doi.org/10.1007/s10965-013-0347-6.

[16] A. Prasad Tiwari, M. Kumar Joshi, J. Lee, B. Maharjan, et al., Heterogeneous electrospun polycaprolactone / polyethylene glycol membranes with improved wettability, biocompatibility, and mineralization, Colloids Surf. A Physicochem. Eng. Asp. 520 (2017) 105–113, https://doi.org/10.1016/j.colsurfa.2017.01.054.

[17] H.T. Bui, O.H. Chung, J. Dela Cruz, J.S. Park, Fabrication and characterization of electrospun curcumin-loaded polycaprolactone-polyethylene glycol nanofibers for enhanced wound healing, Macromol. Res. 22 (2014) 1288–1296, https://doi.org/10.1007/s13233-014-2179-6.

[18] H.R. Bakhsheshi-Rad, A.F. Ismail, M. Aziz, M. Akbari, Z. Hadisi, M. Daroonparvar, X.B. Chen, Antibacterial activity and in vivo wound healing evaluation of polycaprolactone-gelatin methacryloyl-cephalexin electrospun nanofibers, Mater. Lett. 256 (2019) 126618, https://doi.org/10.1016/j.matlet.2019.126618.

[19] N. Liao, A. Rajan Unnithan, M. Kumar Joshi, A. Prasad Tiwari, S. Tshool Hong, Electrospun bioactive poly (ε-caprolactone)– cellulose acetate – dextran antibacterial composite mats for wound dressing applications, Colloids Surf. A Physicochem. Eng. Asp. 469 (2015) 194–201, https://doi.org/10.1016/j.colsurfa.2015.01.022.

[20] J.M. Yousef, E.N. Danial, In vitro antibacterial activity and minimum inhibitory concentration of zinc oxide and nano-particle zinc oxide against pathogenic strains, J Health Sci. 2 (2012) 38–42, https://doi.org/10.5923/j.health.20120204.04.

[21] J. Ruangtong, J. T-Thienprasert, N. Panjaworayan T-Thienprasert, Green synthesized ZnO nanosheets from banana peel extract possess anti-bacterial activity and anti-cancer activity, Mater. Today Commun. 24 (2020) 101224, https://doi.org/10.1016/j.mtcomm.2020.101224.

[22] J. Hussein, M. El-banna, T. Abdel, M.E. El-naggar, Biocompatible zinc oxide nanocrystals stabilized via hydroxyethyl cellulose for mitigation of diabetic complications, Int. J. Biol. Macromol. 107 (2018) 748–754, https://doi.org/10.1016/j.ijbiomac.2017.09.056.

[23] P.K. Mishra, H. Mishra, A. Ekielski, Zinc oxide nanoparticles : a promising nanomaterial for biomedical applications, Drug Discov. Today 22 (2017) 1825–1834, https://doi.org/10.1016/j.drudis.2017.08.006.

[24] K. Kamocki, E. Piva, R.L. Gregory, M.C. Bottino, Development and characterization of novel ZnO-loaded electrospun membranes for, Dent. Mater. 31 (2015) 1038–1051, https://doi.org/10.1016/j.dental.2015.06.004.

[25] R. Augustine, A. Dominic, I. Reju, B. Kaimal, N. Kalarikkal, S. Thomas, Investigation of angiogenesis and its mechanism using zinc oxide nanoparticle-loaded electrospun tissue engineering scaffolds, RSC Adv. 4 (2014) 51528–51536, https://doi.org/10.1039/C4RA07361D.

[26] M. Reza, M. Adel, C. Marlowe, A. Caipang, M.A.O. Dawood, Fish and Shell fish Immunology Immunological responses and disease resistance of rainbow trout (Oncorhynchus mykiss) juveniles following dietary administration of stinging nettle (Urtica dioica), Fish Shellfish Immunol. 71 (2017) 230–238, https://doi.org/10.1016/j.fsi.2017.10.016.

[27] Z. Zekovi, A. Cvetanovi, Š. Jaroslava, S. Gorjanovi, Industrial crops & products chemical and biological screening of stinging nettle leaves extracts obtained by modern extraction techniques, Ind. Crops Prod. 108 (2017) 423–430, https://doi.org/10.1016/j.indcrop.2017.06.055.

[28] Y. Numata, T. Terui, R. Okuyama, N. Hirasawa, Y. Sugiura, I. Miyoshi, T. Watanabe, A. Kuramasu, H. Tagami, H. Ohtsu, The accelerating effect of histamine on the cutaneous wound-healing process through the action of basic fibroblast growth factor, J. Invest. Dermatol. 126 (2006) 1403–1409, https://doi.org/10.1038/sj.jid.5700253.

[29] S. Zenão, A. Aires, C. Dias, M. José, C. Fernandes, Antibacterial potential of Urtica dioica and Lavandula angustifolia extracts against methicillin resistant Staphylococcus aureus isolated from diabetic foot ulcers, J. Herb. Med. 10 (2017) 53–58, https://doi.org/10.1016/j.hermed.2017.05.003.

[30] E. Babaei, M. Hossein Asghari, F. Mehdikhani, M. Moloudizargari, E. Ghobadi, S. Rokhsane Hosseini Pouya, The healing effects of herbal preparations from Sambucus ebulus and Urtica dioica in full-thickness wound models, Asian Pac. J. Trop. Biomed. 7 (2017) 421–427, https://doi.org/10.1016/j.apjtb.2017.01.013.

[31] S. Liu, Y. Kau, C. Chou, J. Chen, R. Wu, W. Yeh, Electrospun PLGA / collagen nanofibrous membrane as early-stage wound dressing, J. Memb. Sci. 355 (2010) 53–59, https://doi.org/10.1016/j.memsci.2010.03.012.

[32] A.C. Queiroz, J.D. Santos, F.J. Monteiro, I.R. Gibson, J.C. Knowles, Adsorption and release studies of sodium ampicillin from hydroxyapatite and glass-reinforced hydroxyapatite composites, Biomaterials. 229 (2001) 1393–1400, https://doi.org/10.1016/S0142-9612(00)00296-9.

[33] T. Ramezani, M. Nabiuni, J. Baharara, K. Parivar, F. Namvar, Sensitization of resistance ovarian cancer cells to cisplatin by biogenic synthesized silver nanoparticles through p53 activation, Iran. J. Pharm. Res. 18 (2019) 222–231.

[34] T. Ohira, O. Yamamoto, Correlation between antibacterial activity and crystallite size on ceramics, Chem. Eng. Sci. 68 (2012) 355–361, https://doi.org/10.1016/j.ces.2011.09.043.

[35] J. Ungula, B.F. Dejene, Effect of solvent medium on the structural, morphological and optical properties of ZnO nanoparticles synthesized by sol-gel method, Phys. B Phys. Condens. Matter. 480 (2016) 26–30, https://doi.org/10.1016/j.physb.2015.10.007.

[36] Z. Karami, I. Rezaeian, P. Zahedi, M. Abdollahi, Preparation and performance evaluations of electrospun poly(ε- caprolactone), poly(lactic acid), and their hybrid (50/50) nanofibrous mats containing thymol as an herbal drug for effective wound healing, J. Appl. Polym. Sci. 129 (2013) 756–766, https://doi.org/10.1002/app.38683.

[37] Z.P. Rad, J. Mokhtari, M. Abbasi, Fabrication and characterization of PCL / zein / gum arabic electrospun nanocomposite sca ff old for skin tissue engineering, Mater. Sci. Eng. C 93 (2018) 356–366, https://doi.org/10.1016/j.msec.2018.08.010.

[38] H. Sama, S. Zamiri, E. Arian, S. Farzam, A. Vaez, Electrospun cellulose acetate / gelatin nanofibrous wound dressing containing berberine for diabetic foot ulcer healing : in vitro and in vivo studies, Sci. Rep. (2020) 1–12, https://doi.org/10.1038/s41598-020-65268-7.

[39] M. Abrigo, S.L. Mcarthur, P. Kingshott, Electrospun nanofibers as dressings for chronic wound care : advances, challenges, and future prospects, Macromol. Biosci. (2014) 1–21, https://doi.org/10.1002/mabi.201300561.

[40] P. Zhang, Y. Zhao, R. Yu, J. Liao, Confined crystallization and degradation of six-arm star PCL with core of cyclotriphosphazene in epoxy thermosets, Eur. Polym. J. 139 (2020) 109989, https://doi.org/10.1016/j.eurpolymj.2020.109989.

[41] N. Haghighipour, An investigation into osteogenic differentiation effects of silk fibroin-nettle (Urtica dioica L.) nanofibers, Int. J. Biol. Macromol. 133 (2019) 795–803, https://doi.org/10.1016/j.ijbiomac.2019.04.165.

[42] R. Augustine, N. Kalarikkal, S. Thomas, R. Augustine, Electrospun PCL membranes incorporated with biosynthesized silver nanoparticles as antibacterial wound dressings, Appl. Nanosci. 6 (2015) 337–344, https://doi.org/10.1007/s13204-015-0439-1.

[43] P. Zahedi, Z. Karami, I. Rezaeian, S.H. Jafari, P. Mahdaviani, A.H. Abdolghaffari, M. Abdollahi, Preparation and performance evaluation of tetracycline hydrochloride loaded wound dressing mats based on electrospun nanofibrous poly (lactic acid)/ poly (-caprolactone) blends, J. Appl. Polym. Sci. 124 (2012) 4174–4183, https://doi.org/10.1002/app.

[44] H. Joodaki, M.B. Panzer, Skin mechanical properties and modeling : a review, Eng. Med. (2018) 1–21, https://doi.org/10.1177/0954411918759801.

[45] M. Pawlaczyk, M. Lelonkiewicz, M. Wieczorowski, Age-Dependent Biomechanical Properties of the Skin, 2013, pp. 302–307, https://doi.org/10.5114/pdia.2013.38359.

[46] R. Augustine, N. Kalarikkal, S. Thomas, Electrospun PCL membranes incorporated with biosynthesized silver nanoparticles as antibacterial wound dressings, Appl. Nanosci. 6 (2016) 337–344, https://doi.org/10.1007/s13204-015-0439-1.

[47] S. Ramakrishna, M. Ramalingam, T.S. Sampath Kumar, W.O. Soboyejo, Biomaterials: A Nano Approach, CRC press, 2016.

[48] E.A. Münchow, M.Tereza P. Albuquerque, B. Zero, K. Kamocki, E. Piva, R.L. Gregory, M.C. Bottino, Development and characterization of novel ZnO-loaded electrospun membranes for periodontal regeneration, Dent. Mater. 31 (2015) 1038–1051, https://doi.org/10.1016/j.dental.2015.06.004.

[49] M. Habibi, I. Je, A. Beitollahi, S. Farhang, J. Hoon, NanoImpact assessment of the potential release of nanomaterials from electrospun nano fi ber fi lter media, NanoImpact 19 (2020), https://doi.org/10.1016/j.impact.2020.100223.

[50] M. Ghorbani, P. Nezhad-mokhtari, S. Ramazani, International journal of biological macromolecules Aloe vera -loaded nano fi brous scaffold based on zein / polycaprolactone / collagen for wound healing, Int. J. Biol. Macromol. 153 (2020) 921–930, https://doi.org/10.1016/j.ijbiomac.2020.03.036.

[51] H. Chen, X. Xing, H. Tan, Y. Jia, T. Zhou, Y. Chen, Zh. Ling, X. Hu, Covalently antibacterial alginate-chitosan hydrogel dressing integrated gelatin microspheres containing tetracycline hydrochloride for wound healing, Mater. Sci. Eng. C 70 (2016) 287–295, https://doi.org/10.1016/j.msec.2016.08.086.

[52] S. Suganya, T.S. Ram, B.S. Lakshmi, V.R. Giridev, Herbal drug incorporated antibacterial nanofibrous mat fabricated by electrospinning : an excellent matrix for wound dressings, J. Appl. Polym. Sci. 121 (2011) 2893–2899, https://doi.org/10.1002/app.

[53] W. Zhang, S. Ronca, E. Mele, Electrospun nanofibres containing antimicrobial plant extracts, Nanomaterials 7 (2017) 42, https://doi.org/10.3390/nano7020042.

[54] A. Khezerlou, M. Alizadeh-Sani, M. Azizi-Lalabadi, A. Ehsani, Nanoparticles and their antimicrobial properties against pathogens including bacteria, fungi, parasites and viruses, Microb. Pathogen. 123 (2018) 505–526, https://doi.org/10.1016/j.micpath.2018.08.008.

[55] J.G. Merrell, S.W. Mclaughlin, L. Tie, C.T. Laurencin, A.F. Chen, L.S. Nair, Curcumin-loaded poly (e -caprolactone) nanofibres : diabetic wound dressing with anti-oxidant and anti-inflammatory properties, Clin. Exp. Pharmacol. Physiol. 36 (2009) 1149–1156, https://doi.org/10.1111/j.1440-1681.2009.05216.x.

[56] J. Chen, Y. Huang, X. Ma, Y. Lei, Functional self-healing materials and their potential applications in biomedical engineering, Adv. Compos. Hybrid Mater. 1 (2018) 94–113, https://doi.org/10.1007/s42114-017-0009-y.